



Synthesis, crystal structures, fluorescence, electrochemiluminescent properties, and Hirshfeld surface analysis of four Cu/Mn Schiff-base complexes

Yumei Zeng¹ | Haiyang Zhang¹ | Yujie Zhang¹ | Fanghua Ji¹ | Jinlu Liang² | Shuhua Zhang^{1,3}

¹College of Chemistry and Bioengineering, Guangxi Key Laboratory of Electrochemical and Magnetochemical Functional Materials, Guilin University of Technology, Guilin, 541004, People's Republic of China

²College of Petroleum and Chemical Engineering, Beibu Gulf University, Qinzhou, 535011, People's Republic of China

³College of Chemistry, Guangdong University of Petrochemical Technology, Maoming, Guangdong, 525000, People's Republic of China

Correspondence

Shuhua Zhang, College of Chemistry, Guangdong University of Petrochemical Technology, Maoming, Guangdong 525000, People's Republic of China.
Email: zsh720108@163.com

Fanghua Ji and Shuhua Zhang, College of Chemistry and Bioengineering, Guangxi Key Laboratory of Electrochemical and Magnetochemical Functional Materials, Guilin University of Technology, Guilin, 541004, People's Republic of China.
Email: fanghuaji@glut.edu.cn; zsh720108@163.com

Jinlu Liang, College of Petroleum and Chemical Engineering, Beibu Gulf University, Qinzhou, 535011, People's Republic of China.
Email: ljinlu@163.com

Funding information

Collaborative Innovation Center for Exploration of Hidden Nonferrous Metal Deposits and Development of New Materials in Guangxi, Grant/Award Number: GXYSXTZX2017-II-3; the Nature Science Foundation of China, Grant/Award Number: 21861014

Abstract

Four new complexes $[\text{Cu}(\text{L}^1)_2]_n$ (**1**), $[\text{Mn}(\text{L}^1)_2]_n$ (**2**), $[\text{Cu}(\text{L}^2)_2]_n$ (**3**), $[\text{Mn}(\text{L}^2)_2]_n$ (**4**), $\text{HL}^1 = 2-\text{(((4H-1,2,4-triazol-4-yl)imino)methyl)-4,6-dichlorophenol}$; $\text{HL}^2 = 2-\text{(((4H-1,2,4-triazol-4-yl)imino)methyl)-4,6-dibromophenol}$ were synthesized by microreaction bottle method. Complexes **1** and **3** and **2** and **4** are isomorphous heterostructures having the same molecular structure. The structures of **1–4** were characterized using single X-ray diffraction, Fourier-transform infrared spectroscopy, powder X-ray diffraction, and thermogravimetric analysis, and their potential applications were analyzed by detecting their fluorescence and electrochemical luminescence (ECL). Hirshfeld surface analysis indicates that $\text{X}\cdots\text{H}$ ($\text{X} = \text{Br}, \text{Cl}$) interactions play a crucial role in stabilizing the self-assembly process of **1–4**, which show highly intense ECL in *N,N*-dimethylformamide solution and high thermal stability.

KEY WORDS

electrochemical luminescence, fluorescence, polymer, Schiff-base

1 | INTRODUCTION

The design and synthesis of novel coordination polymer (CP) materials with Schiff base as an organic ligand have been the hot topic of current research,^[1–3]

as they have wide applications in optics,^[4–6] electromagnetism,^[7–9] adsorption,^[10] and catalysis.^[11–15] Currently, the main coordination modes of Schiff bases are the coordination of metal ions with O and N.^[16–20] Therefore, the choice of an organic ligand determines

the nature of the CPs. 1,2,4-Triazole ligand and its derivatives can bridge transition metal ions through the N–M coordination mode to obtain high-nuclear compounds and their CPs having unique properties. 3-Amino-1,2,4-triazole was selected as an organic bridging ligand by Hyunsoo Park, to form four new CPs with Zn.^[19] Yun Gong and his colleagues used 4-amino-4H-1,2,4-triazole and its derivative 3,5-dimethyl-4-amino-4H-1,2,4-triazole as the main ligands and combined them with Cu and Ag to form 1D–3D metal organic framework materials. Cu compounds exhibited better electrocatalytic activity in generating H₂ from water.^[17] In this study, 4-amino-4H-1,2,4-triazole was combined with 3,5-dichloro-2-hydroxybenzaldehyde or 3,5-dibromo-2-hydroxybenzaldehyde to form a C=N bond by an aldehyde-amino-group condensation reaction. The ligands were coordinated with metal ions (Cu^{II}, Mn^{II}) under certain conditions to obtain CPs. That is, four CPs with Cu^{II} and Mn^{II} as metal centers were synthesized. Their structures were characterized using single crystal X-ray diffraction, elemental analysis, infrared (IR) spectroscopy, and thermogravimetric analysis.

Electrochemical luminescence (ECL) materials are now being used in areas of professional field due to their low background noise and highly sensitive electrochemical response signals.^[21] The ECL process uses a certain pulse of electrical signals to stimulate the excitation energy of the material and then generates energy radiation with a certain electrical signal.^[22] The most common solution is to prepare composite materials, and generally Ru(II) and Ir(II) are suitable metals for the preparation of CPs.^[21–24] All of the previous methods are expensive and involve complicated experimental procedures. But our synthetic Schiff-base raw materials and metal salts are both low cost and efficient.

Hirshfeld surface analysis can explain the fundamental issue in a material design process from a certain angle and is widely used as a unique method for analyzing intermolecular interactions,^{25–27} using the 2D fingerprint map. It has also concentrated on the Hirshfeld surface analysis in the following research. Fluorescent CP materials can be used to detect the specific recognition of specific ions, organisms, or cancer cells because of their strong and stable fluorescent properties, large specific surface area, and structural controllability.^[28] Moreover, the excellent fluorescent luminescence properties of CPs are not so dependent on external conditions and usually exhibit good fluorescence intensity at room temperature.^[28,29] Another major factor is that the four new complexes

are not the electron transfer resulting from the original *d*-*d* transition but the electron transfer between the ligand and the metal (LMCT).^[30,31] The fluorescence measurement of the four complexes revealed that the four complexes had different degrees of red-shift than the maximum fluorescence intensity of the ligands: complexes **1** and **2** having red-shifts about 44–57 nm and complexes **3** and **4** having red-shifts about 7–10 nm. In addition to the effect of the C=N bond on the fluorescent properties of the complexes in Schiff bases, it is reasonable to assume that halogen atoms in salicylaldehyde may cause fluorescence quenching.

2 | EXPERIMENTAL

2.1 | Materials and instrumentation

All chemicals were commercially available and used as received without further purification. The crystal structures were determined using SuperNova (single source at offset, Eos, Agilent Technologies, Palo Alto, America) diffractometer and SHELXL crystallographic software of molecular structures. FT-IR spectra were recorded from KBr pellets in the range of 4000 to 400 cm⁻¹ on a Nicolet Nexus 470 FT-IR infrared spectrometer (Nicolet, American). The PXRDs of 1–4 were determined by a X'Pert³ Powder X-ray powder diffractometer (Panaco, Netherlands). TGA measurements were carried out with heating the crystalline sample from 25 to 900 °C at a rate of 10 °C·min⁻¹ in N₂ atmosphere on a SDT Q600 Thermogravimetric Analyzer (TA, American). ECL properties and cyclic voltammetry (CV) of compounds 1–4 in N,N-dimethylformamide(DMF) solution were studied using MPI-E Electrochemiluminescence Analysis System (Xi'an Ruimai Analytical Instrument Co., Ltd. Xi'an, China).

2.2 | Syntheses

2.2.1 | Synthesis of HL¹

A mixture of 3,5-dichloro-2-hydroxybenzaldehyde (1.91 g, 10 mmol), 4H-4-amino-1,2,4-triazole (taya, 0.84 g, 10 mmol), and ethanol (20 ml) in a 100 ml three-necked flask was refluxed at 80°C for 120 min. The color of the solution changed to brown and was enriched at 80°C for 2 h. A brown power was obtained by filtration, washed with hot ethanol (10 ml × 3), and dried in an oven at 50°C for 24 h (yield: 2.468 g, ca. 96%, based on taya). Analysis calculated (%) for

HL^1 , $\text{C}_9\text{H}_6\text{Cl}_2\text{N}_4\text{O}$ ($M_r = 257.08$): C, 42.05; H, 2.35; N, 21.79. Found: C, 41.98; H, 2.42; N, 21.85. The IR data of HL^1 (KBr, cm^{-1} , see Figure S1 in the supporting information): 3438 m, 3130 m, 1660 w, 1597 s, 1515 s, 1465 s, 1377 m, 1327 s, 1245 s, 1176 m, 1056 s, 868 m, 723 m, 641 w.

2.2.2 | Synthesis of HL^2

The method of synthesizing HL^2 is similar to that of synthesizing HL^1 , except that 3,5-dichloro-2-hydroxybenzaldehyde was replaced by 3,5-dibromosalicylaldehyde. A brown powder was obtained by filtration, washed with ethanol (10 ml \times 3), and dried in an oven at 50°C for 24 h (yield: 3.356 g, ca 97%, based on taya). Analysis calculated (%) for HL^2 : $\text{C}_9\text{H}_6\text{Br}_2\text{N}_4\text{O}$ ($M_r = 345.98$): C, 31.24; H, 1.75; N, 16.19. Found: C, 31.18; H, 1.82; N, 16.25. The IR data of HL^2 (KBr, cm^{-1} , see Figure S1 in the supporting information): 3450 s, 3124 m, 3067 m, 1634 w, 1515 s, 1452 m, 1364 s, 1307 s, 1232 s, 1176 s, 1062 s, 962 m, 868 s, 730 m, 623 w.

2.2.3 | Synthesis of $[\text{Cu}(\text{L}^1)_2]_n$ (1)

HL^1 (0.051 g, 0.2 mmol) was added to a clean 25 ml small glass bottle. DMF (5 ml) was poured into the glass bottle. At the same time, $\text{Cu}(\text{AcO})_2 \cdot \text{H}_2\text{O}$ (0.040 g, 0.2 mmol) was dissolved in 5 ml of deionized water. The two solutions were then mixed and stirred in the glass bottle for 20 min. Then, the magneton was sucked out by a magnet, the glass bottle was sealed and placed in an oven at 90°C, and blue block crystals were obtained after 3 days. The reaction product was washed with heated DMF (10 ml \times 3) and double-distilled water (10 ml \times 3). Blue block crystals of **1** were obtained (yield: 0.065 g, ca 56.3%, based on HL^1). Analysis calculated (%) for **1**, $\text{C}_{18}\text{H}_{10}\text{Cl}_4\text{CuN}_8\text{O}_2$ ($M_r = 575.68$): C, 37.56; H, 1.75; N, 19.46. Found: C, 37.48; H, 1.81; N, 19.53. The IR data of **1** (KBr, cm^{-1} , see Figure S1 in the supporting information): 3111 m, 1597 s, 1509 m, 1440 s, 1314 w, 1214 m, 1157 m, 1069 s, 849 w, 768 m, 657 w.

2.2.4 | Synthesis of $[\text{Mn}(\text{L}^1)_2]_n$ (2)

The ratio of the metal salt to the ligand was the same as **1**, but $\text{Mn}(\text{AcO})_2 \cdot 4\text{H}_2\text{O}$ was dissolved in dimethyl sulfoxide (DMSO) and stirred for 20 min. Then, 5 ml of double-distilled water was added, and the reaction flask was sealed and placed in an oven at 80°C. Red block crystals

of **2** were obtained (yield: 0.066 g, ca 58.1%, based on HL^1). Analysis calculated (%) for **2**, $\text{C}_{18}\text{H}_{10}\text{Cl}_4\text{MnN}_8\text{O}_2$ ($M_r = 567.07$): C, 38.13; H, 1.78; N, 19.76. Found: C, 38.10; H, 1.82; N, 19.79. The IR data of **2** (KBr, cm^{-1} , see Figure S1 in the supporting information): 3143 m, 1603 m, 1515 w, 1465 s, 1346 w, 1214 m, 1163 m, 1057 s, 855 w, 761 m, 629 w.

2.2.5 | Synthesis of $[\text{Cu}(\text{L}^2)_2]_n$ (3)

Compound **3** was prepared in a similar way as **1**, except that HL^1 was replaced with HL^2 . Blue bulk crystals of **3** were obtained (yield: 0.080 g, ca 51.2%, based on HL^2). Analysis calculated (%) for **3**, $\text{C}_{18}\text{H}_{10}\text{Br}_4\text{CuN}_8\text{O}_2$ ($M_r = 753.49$): C, 28.69; H, 1.34; N, 14.82. Found: C, 28.66; H, 1.37; N, 14.85. The IR data of complex **3** (KBr, cm^{-1} , see Figure S1 in the supporting information): 3117 m, 1591 s, 1509 m, 1433 s, 1314 w, 1207 m, 1157 m, 1062 s, 962 w, 843 m, 761 s, 623 m.

2.2.6 | Synthesis of $[\text{Mn}(\text{L}^2)_2]_n$ (4)

Compound **4** was prepared in a similar way as **2**, except that HL^1 was replaced with HL^2 . Red square crystals of **4** were obtained (yield: 0.039 g, ca 52.4%, based on HL^2). Analysis calculated (%) for **4**, $\text{C}_{18}\text{H}_{10}\text{Br}_4\text{MnN}_8\text{O}_2$ ($M_r = 744.88$): C, 29.03; H, 1.35; N, 15.04. Found: C, 29.01; H, 1.38; N, 15.09. The IR data of complex **4** (KBr, cm^{-1} , see Figure S1 in the supporting information): 3130 m, 1591 s, 1509 m, 1459 s, 1370 w, 1226 m, 1151 m, 1056 s, 987 w, 855 w, 755 w, 704 m, 610 w.

2.3 | Crystal structure determination

The diffraction data were collected on a SuperNova with graphite monochromated Mo-K α radiation ($\lambda = 0.71073 \text{ \AA}$) at $16 \pm 1^\circ\text{C}$ by using the ω scan mode in the ranges $2.94^\circ \leq \theta \leq 25.24^\circ$ (**1**), $2.88^\circ \leq \theta \leq 25.01^\circ$ (**2**), $3.07^\circ \leq \theta \leq 25.24^\circ$ (**3**), and $2.86^\circ \leq \theta \leq 25.24^\circ$ (**4**). The raw frame data were integrated with the SAINT program. The structures of **1–4** were determined by direct methods using SHELXT and refined by full-matrixleast-squares on F^2 using SHELXL-2015 within the OLEX-2 GUI.^[32] An empirical absorption correction using spherical harmonics was implemented in SCALE3 ABSPACK scaling algorithm. All non-hydrogen atoms were refined anisotropically. All hydrogen atoms were positioned geometrically and refined using a riding model. Calculations and graphics were performed using SHELXTL.^[33,34] Computer programs used were CrysAlis PRO, Agilent

TABLE 1 Crystallographic data for complexes 1–4

Complexes	1	2	3	4
Formula	C ₁₈ H ₁₀ Cl ₄ CuN ₈ O ₂	C ₁₈ H ₁₀ Cl ₄ MnN ₈ O ₂	C ₁₈ H ₁₀ Br ₄ CuN ₈ O ₂	C ₁₈ H ₁₀ Br ₄ MnN ₈ O ₂
M _r	575.68	567.07	753.49	744.88
Crystal size (mm)	0.20 × 0.19 × 0.13	0.21 × 0.17 × 0.12	0.14 × 0.13 × 0.11	0.21 × 0.18 × 0.14
Crystal system	Monoclinic	Tetragonal	Monoclinic	Tetragonal
Space group	P2 ₁ /c	P4 ₁ 2 ₁ 2	P2 ₁ /c	P4 ₁ 2 ₁ 2
a (Å)	12.1734(5)	7.6879(2)	12.6988(9)	7.7367(2)
b (Å)	8.5038(5)	7.6879(2)	8.7060(5)	7.7367(2)
c (Å)	10.4456(5)	35.9055(13)	10.4404(6)	36.6885(16)
α (°)	90.00	90.00	90.00	90.00
β (°)	101.328(4)	90.00	101.410(7)	90.00
γ (°)	90.00	90.00	90.00	90.00
V (Å ³)	1060.27(9)	2122.13(14)	1131.43(13)	2196.07(17)
F(000)	574	1132	718	1420
Z	2	4	2	4
D _c (g cm ⁻³)	1.803	1.775	2.212	2.253
μ (mm ⁻¹)	1.57	1.162	8.063	7.915
θ range (°)	2.94–25.24	2.88–25.24	3.07–25.24	2.86–25.24
Ref. meas./indep.	4274/2164	21173/1984	4519/2332	4853/2161
Obs. ref. [I > 2σ(I)]	1435	1984	1733	1908
R _{int}	0.0425	0.0314	0.0324	0.0285
R ₁ [I ≥ 2σ(I)] ^a	0.0595	0.0513	0.0510	0.0369
ωR ₂ (all data) ^b	0.1653	0.1303	0.1269	0.0639
Goof	0.978	0.0994	1.021	1.062
Δρ (max, min) (eÅ ⁻³)	0.981, -0.894	0.300, -0.351	1.604, -1.108	0.486, -0.404

^aR₁ = Σ||F_o|−|F_c||/Σ|F_o|.^bwR₂ = [Σw(|F_o²|−|F_c²|)²/Σw(|F_o²|)²]^{1/2}.

Technologies, Version 1.171.37.35, SHELXL-15,^[33,34] and Olex2.^[32] The crystallographic details for **1–4** are provided in Table 1. Selected bond lengths and angles for **1–4** are listed in Table 2.

3 | RESULT AND DISCUSSION

3.1 | Description of the crystal structures

3.1.1 | Crystal structures description of 1 and 3

Single crystal X-ray diffraction analysis revealed that **1** and **3** were isomeric complexes (Figure 1), and the crystal system (monoclinic) and space group (P2₁/c) of **1** and **3** were identical. Therefore, only complex **1** was analyzed.

Complex **1** crystallized in the monoclinic space group P2₁/c. As shown in Figure 1, Cu²⁺ as a central metal ion coordinated with two oxygen atoms (O1, O1ⁱ) and four nitrogen atoms (N4, N4ⁱ, N2ⁱⁱ, N2ⁱⁱⁱ) provided by four L¹ ligands to form a hexacoordinated octahedral CuN₄O₂ coordination configuration. The bond distances of Cu1–O1, Cu1–N4, and Cu1–N2ⁱⁱ (symmetry code: (ii) x, −y − 0.5, z + 0.5) were 1.947(3), 2.344(4), and 2.049(4) Å, respectively. Note that the bond length difference around Cu1 may have been caused by the Jahn–Teller effect^[35–37] and that the L ligand displayed the μ₂–L–κ³O¹,N¹,N² coordination mode (Figure 1), which is different from the coordination mode of [Cu(TMP)₂(H₂O)₂] (HTMP is (E)-2-(((4H-1,2,4-triazol-4-yl)imino)methyl)-6-methoxyphenol, μ₁–TMP–κ²O¹,N¹ coordination mode).^[37] Further, the one coordination atom (N1) of the L ligand was not involved in coordination. In the ac plane, O1, O1ⁱ, N4, N4ⁱ, and Cu1 atoms were on

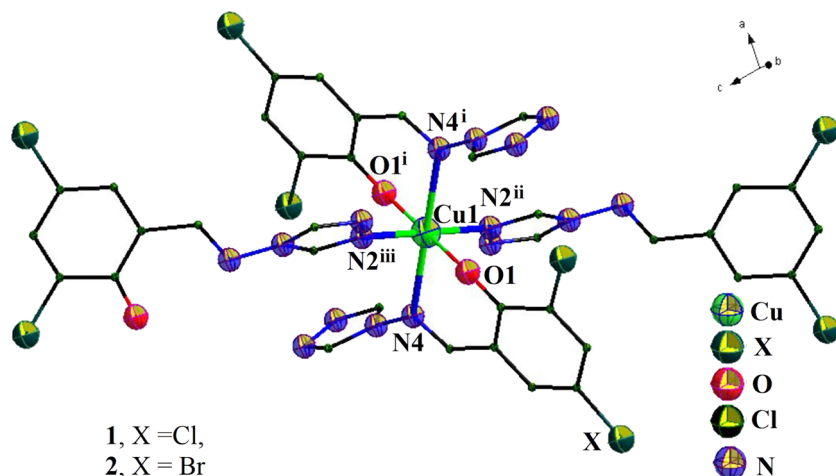
TABLE 2 Selected bond length (Å) and bond angle (°) of 1–4

Complexes	1	2	3	4
M1–O1 ⁱ	1.947(3)	2.052(3)	1.941(5)	2.049(4)
M1–O1	1.947(3)	2.053(3)	1.941(5)	2.049(4)
M1–N4	2.344(4)	2.378(4)	2.384(6)	2.408(4)
M1–N4 ⁱ	2.344(4)	2.378(4)	2.384(6)	2.408(4)
M1–N2 ⁱⁱ	2.049(4)	2.248(5)	2.048(6)	2.252(5)
M1–N2 ⁱⁱⁱ	2.049(4)	2.248(5)	2.048(6)	2.252(5)
O1–M1–O1 ⁱ	180.00(16)	165.0(2)	180.0(3)	164.5(2)
O1–M1–N4	82.08(13)	78.11(14)	80.7(2)	78.34(15)
O1 ⁱ –M1–N4	97.91(13)	92.67(15)	99.3(2)	92.02(15)
O1–M1–N4 ⁱ	97.91(13)	92.67(15)	99.3(2)	92.02(15)
O1 ⁱ –M1–N4 ⁱ	82.09(13)	78.11(14)	80.7(2)	78.34(15)
O1–M1–N2 ⁱⁱ	88.96(14)	86.02(15)	89.2(2)	87.80(16)
O1–M1–N2 ⁱⁱⁱ	91.04(14)	105.41(16)	90.8(2)	103.99(16)
O1 ⁱ –M1–N2 ⁱⁱⁱ	88.96(14)	86.02(15)	89.2(2)	87.80(16)
O1 ⁱ –M1–N2 ⁱⁱ	91.04(14)	105.41(16)	90.8(2)	103.99(16)
N4 ⁱ –M1–N4	180.0	104.9(2)	180.0	103.8(2)
N2 ⁱⁱⁱ –M1–N4	93.88(15)	88.73(16)	94.5(2)	88.81(17)
N2 ⁱⁱ –M1–N4 ⁱ	93.88(15)	88.73(16)	94.5(2)	88.81(17)
N2 ⁱⁱ –M1–N4	86.12(15)	159.39(15)	85.5(2)	161.42(17)
N2 ⁱⁱⁱ –M1–N4 ⁱ	86.12(15)	159.39(15)	85.5(2)	161.42(17)
N2 ⁱⁱ –M1–N2 ⁱⁱⁱ	180.0	82.8(2)	180.0	82.6(3)

Symmetry codes: (i) $-x + 1, -y, 1 - z$; (ii) $x, -y - 0.5, z + 0.5$; (iii) $-x + 1, y + 0.5, 0.5 - z$. (i) $y - 1, x + 1, -z - 1$; (ii) $x, y + 1, z$; (iii) $y, x + 1, -z - 1$. (i) $2 - x, -y, 1 - z$; (ii) $x, -y - 0.5, z - 0.5$; (iii) $-x + 2, y + 0.5, 1.5 - z$. (i) $y, x, 1 - z$; (ii) $x - 1, y, z$; (iii) $y, x - 1, 1 - z$.

the same plane (the plane equation is $1.6888x + 7.0731y + 5.2207z = 7.8357$) because the bond angles of O1–Cu1–O1ⁱ and N4–Cu1–N4ⁱ were also 180°. As the atoms in the Cu-coordinated octahedral environment were derived from different ligand groups in four directions, the steric hindrance of each atom was different, which resulted in a twisted octahedral coordination configuration of copper ions.

As shown in Figure S2a, each L ligand served as a bridge to link two adjacent Cu(II) ions and form a staircase-shaped chain. The length of the step in the staircase-shaped chains was 10.96 and 10.94 Å for **1** and **3**, respectively, which was made up of two 4-amino-4H-1,2,4-triazole groups of the L ligands and one Cu ion. The height of the step in the staircase-shaped chains was 4.680 and 4.751 Å for **1** and **3**, respectively, which is the

**FIGURE 1** Molecule structures of **1** and **3**

distance N4...N4ⁱ (symmetry code: (i) $-x + 1, -y, -z + 1$ for **1**; 2 - $x, -y, 1 - z$ for **3**). The N4...N4ⁱ...N4B angle was 112.4° and 114.08° for **1** and **3**, respectively (symmetry code (B) for **1**: 1 - $x, -1 - y, -z$; for **3**: $x, 1 + y, z - 1$). One-dimensional chains in different directions formed 2D networks by sharing copper atoms (Figure S2b). The N4...Cu1...N4ⁱⁱⁱ angle was 84.40° and 85.26° for **1** and **3**, respectively (symmetry code (iii) for **1**: 1 - $x, 0.5 + y, 0.5 - z$; for **3**: 2 - $x, 0.5 + y, 1.5 - z$). As a result, a rectangular gap was formed in the 2D plane (Figure S2c). The 2D network structure was stacked along the a -axis direction with a layer spacing of 12.439 Å to form a 3D structure with the X- π (for **1**: Cl₂- π ^e, 3.428(1) Å, symmetry code: (e) 2 - $x, y - 0.5, 1.5 - z$; for **3**: Br₂- π ^f, 3.277(1) Å, symmetry code: (f) 1 - $x, y - 0.5, 0.5 - z$, Figure S2d).

3.1.2 | Crystal structures description of **2** and **4**

Single crystal X-ray diffraction analysis revealed that **2** and **4** were isomeric complexes (Figure 2), and the crystal system (tetragonal) and space group ($P4_12_12$) of **2** and **4** were identical. Therefore, only complex **2** was analyzed.

The metal coordination of **2** and **4** was similar to that of **1** and **3**, but the ligands stretched in different directions in space. For **1** and **3**, the two μ_1 -L- κ^2 O¹,N¹ bidentate ligands are center symmetrical with the copper atom as the center of symmetry. O1-N4-Cu1-N4ⁱ-O1ⁱ five atoms formed one plane (Figure 3a). N2ⁱⁱ and N2ⁱⁱⁱ coordinated with copper atoms from above and below this plane, respectively. Copper atoms formed a perfect octahedral configuration (Table 2). The bond angles of

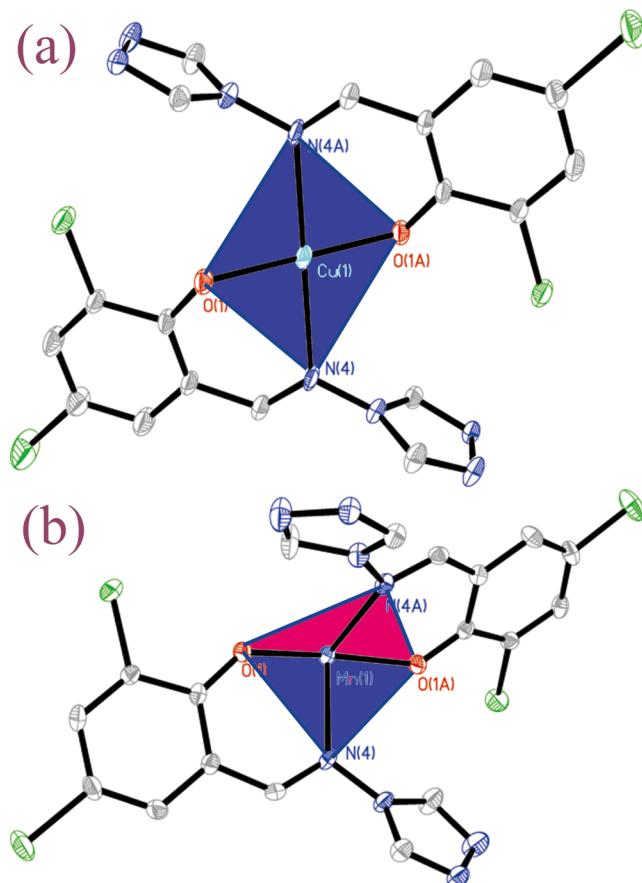


FIGURE 3 Polyhedron of MO₂N₂ contrast for (a) **1** and (b) **2**

O1-Cu1-O1ⁱ and N4-Cu1-N4ⁱ were 180°; for **2** and **4**, the two μ_1 -L- κ^2 O¹,N¹ bidentate ligands with the Cu ion constructed an obviously distorted tetrahedron (seesaw-shaped) (Figure 3b). The bond angles of O1-Mn1-O1ⁱ

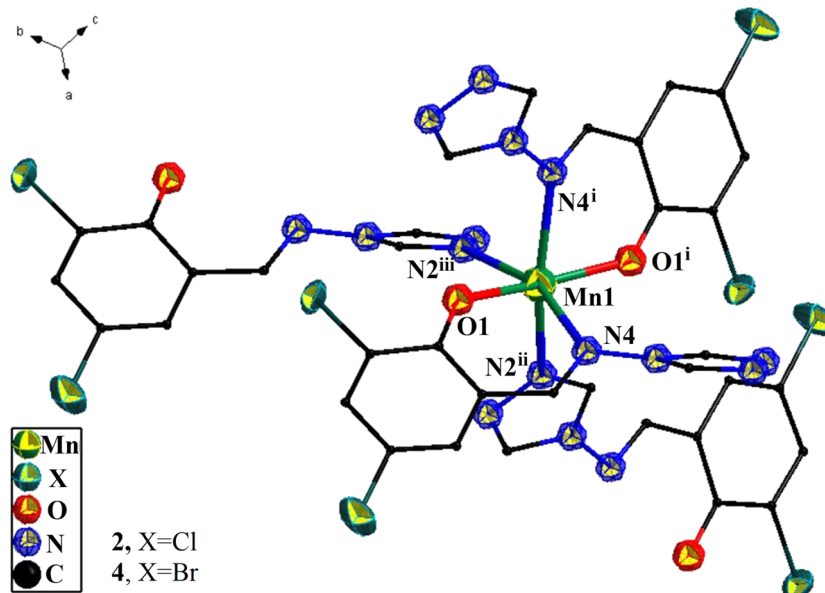
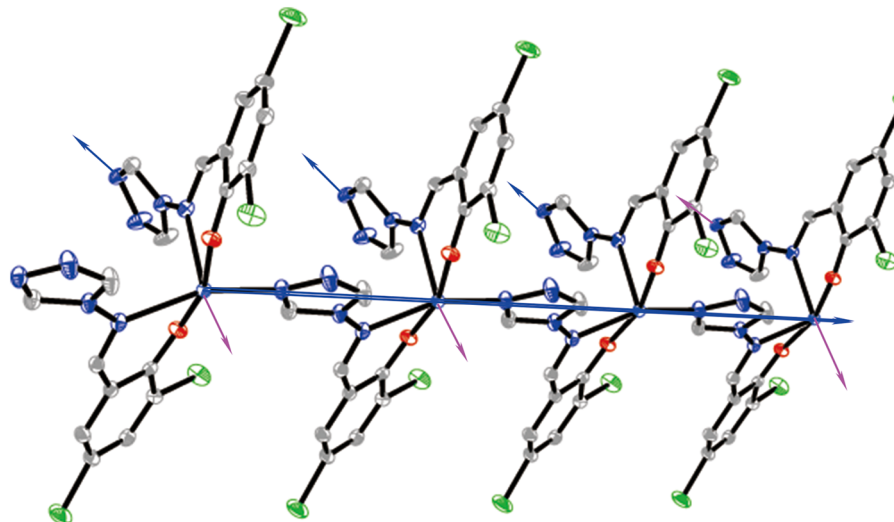


FIGURE 2 Molecule structures of **2** and **4**

FIGURE 4 1D chain of **2** and **4**

and N4–Mn1–N4ⁱ were 165.0(2) $^{\circ}$ and 104.9(2) $^{\circ}$, respectively (symmetry code: (i) $y - 1, x + 1, -z - 1$ for **2**). In **2** and **4**, the other two coordination sites were adjacent in the distorted octahedron.

Mn1 coordinated with two oxygen atoms (O1, O1ⁱ) and four nitrogen atoms (N4, N4ⁱ, N2ⁱⁱ, N3ⁱⁱⁱ) provided by four different L ligands, and formed a slightly distorted octahedral MnN₄O₂ coordination configuration. The bond distances of Mn1–O1, Mn1–N4, and Mn1–N2ⁱⁱ (symmetry code: (ii) $x, y + 1, z$) were 2.053(3), 2.378(4), and 2.248(5) Å, respectively. The mononuclear Mn(L¹)₂ unit constructed a 1D chain through an Mn–N coordination bond which is different from the staircase-shaped chain of **1** and **3**. In the 1D chain of **2** and **4**, manganese atoms were in a straight line while the Mn1…Mn1a distance was 7.688(1) Å (Figure 4). The 1D chain further constructed a 2D lattice through Mn–N2 and N2–Mn bonds. The distance adjacent to the 1D chain was 7.688(1) Å. As a result, there is a square lattice of 7.668 × 7.688 Å and 7.737 × 7.737 Å on the plane for **2** and **4**, respectively (Figure S3a), which is different from the rectangular gap of **1** and **3**. The 2D lattice formed 3D supramolecular network through the X…X interaction (for **2**: Cl2…Cl2E, 3.623(1) Å, symmetry code: (E) $-1 - y, -1 - x, -1.5 - z$; for **4**: Br2…Br2F, 3.738(1) Å, symmetry code: (F) $1 - y, 1 - x, 1.5 - z$) and C–H…N hydrogen bonds (for **2**: C7–H7…N1G, 3.388(1) Å, symmetry code: (G) $y - 0.5, -0.5 - x, 1.75 + z$; for **4**: C7–H7…N1G, 3.419(1) Å, symmetry code: (G) $0.5 - y, x - 0.5, 0.25 + z$, Figure S3b).

3.2 | IR spectrum

The IR spectral data of the ligand HL^{1&2} and compounds **1–4** are shown in Figure S1. All the characteristic groups

of a series of compounds exhibited obvious absorption peaks as shown in the IR spectrum. The ligands HL^{1&2} showed a *br* absorption band at 3448–3450 cm⁻¹(O–H), because of the stretching vibration adsorption peak of crystal water molecules in the air or in the complexes.^[18] Bands at 1660 and 1634 cm⁻¹ are attributed to the Schiff base imine group –CH=N– of the free HL¹ and HL², respectively, which red-shifted to 1597, 1603, 1591, 1591 cm⁻¹ for **1–4**, respectively. The results indicate that the nitrogen atom of the –CH=N– group in L ligands was coordinated.^[37–39] The C–O stretching vibrations of the free HL ligands at 1245 and 1232 cm⁻¹ for free HL¹ and HL², respectively, red-shifted to 1214, 1214, 1207, and 1226 cm⁻¹ for **1–4**, respectively, suggesting its participation in chelation.^[35,40] The bands at 3130, 3124, 3111, 3143, 3117, and 3130 cm⁻¹ for HL¹, HL², **1–4**, respectively, are attributed to the weak C–H stretching vibration of the benzene ring, while those at 868, 868, 849, 855, 843, and 855 cm⁻¹ for HL¹, HL², **1–4**, respectively, are attributed to the C–X (X = Cl or Br) stretching vibration. By comparing the IR spectrum of the HL¹ and HL² ligands with that of the complexes **1–4**, we find that the change in the IR spectrum may have been due to the change in the density of the electron cloud around the ligand molecule after the ligands were coordinated to the metal ions.

3.3 | Thermal stability analysis

Under the test conditions of N₂ flow rate of 100.0 ml/min and heating rate of 10°C/min, the thermal stability of complexes **1–4** was tested from room temperature to 900°C (PXRD has been proven to be a pure phase sample, Figure S4). Thermogravimetric curves of complexes **1–4** are shown in Figure 5. The four complexes exhibited

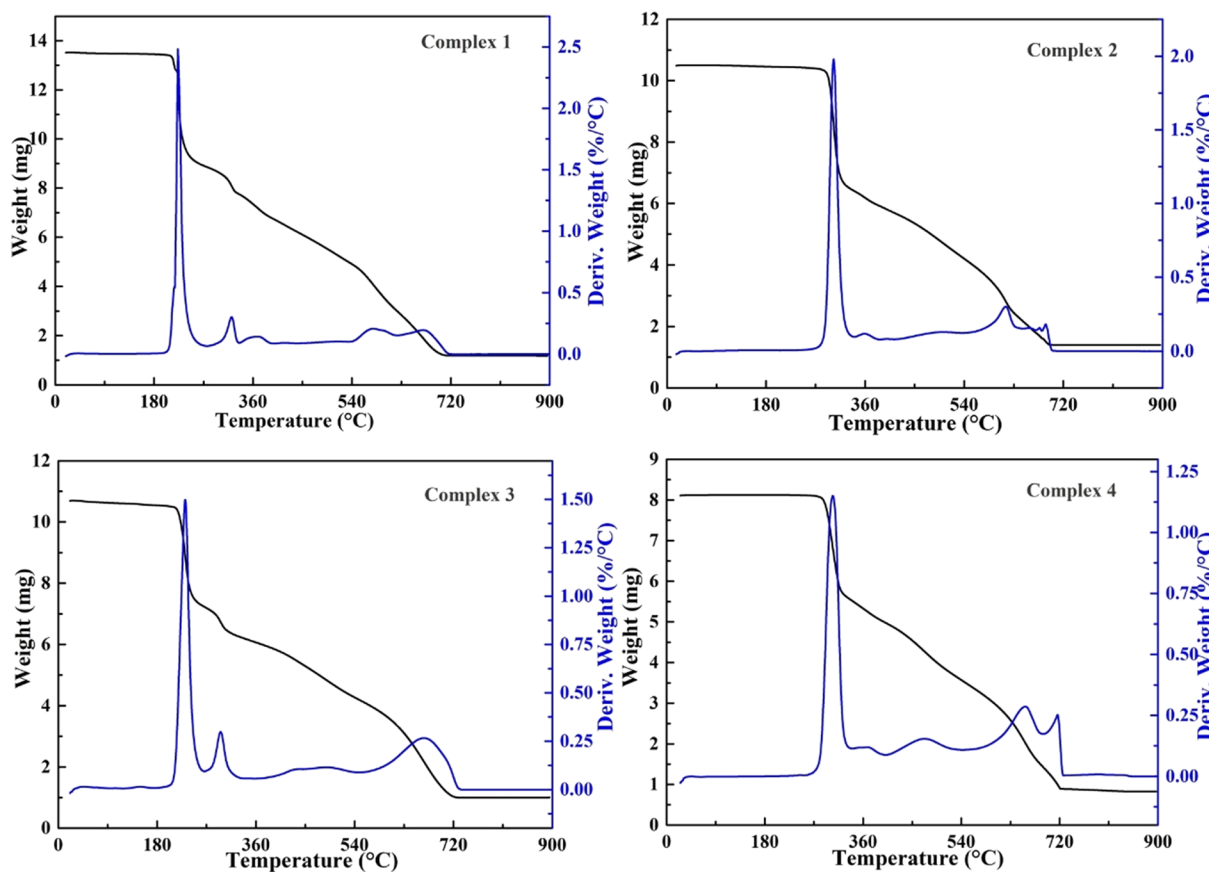


FIGURE 5 Thermogravimetric curves of **1–4**

extremely similar weightlessness behaviors, with complexes **1** and **3**, and **2** and **4** being slightly different in subtleties. Complexes **2** and **4** began to decompose at about 329°C, while complexes **1** and **3** began to collapse at about 220°C, which indicates that **2** and **4** are more stable than **1** and **3**. The decomposition end temperature was about 720°C, and the remaining products were the corresponding metal oxides.

3.4 | Hirshfeld surface analysis

Through the Hirshfeld analysis of the surface effect of the structural unit, we obtained the 2D fingerprint as shown in Figure 6. The properties and types of intermolecular interactions within the crystal were quantitatively analyzed, and the work of this part was calculated using the CrystalExplorer 3.1 program.^[41] The acting forces between different elements were studied separately in the 2D fingerprint, and then the ratio of the forces of the various parts to research with the structure was analyzed. For compounds **1–4**, X (Cl and Br)-H accounts for a large proportion of the entire 2D fingerprint, 21.2%, 16.5%, 20.9%, and 17.0%, respectively. The interaction between the

intramolecular X (Cl and Br) and the extramolecular H is indicated in the fingerprint region of the lower-left corner (donor) of the fingerprint. The interaction of H inside the molecule with the X (Cl and Br) outside the molecule was in the lower-right corner (receptor) fingerprint area, indicating a clear C-H…X (Cl and Br) nonconventional hydrogen bond in the crystal structure of the compounds **1–4**. The interaction C-X(Cl and Br) also plays an important role in the total 2D fingerprint. The percentage of C-X(Cl and Br) in compounds **1–4** was 12.7%, 13.4%, 12.8%, and 15.1%, respectively. The shortest C…X distances were 3.501, 3.408, 3.533, and 3.397 Å for **1–4**, respectively. Another major intermolecular interaction of **1–4** was the H-H interaction, which is reflected in the middle of the scattering point of the 2D fingerprint (the percentage of H-H effect of compounds **1–4** was 13.4%, 10.7%, 12.7%, and 10.6%). The forces of different elements are summarized in Table 3.

3.5 | Fluorescent properties of **1–4**

The luminescent properties of compounds **1–4** and the free HL^{1&2} ligands were investigated in DMF solvent

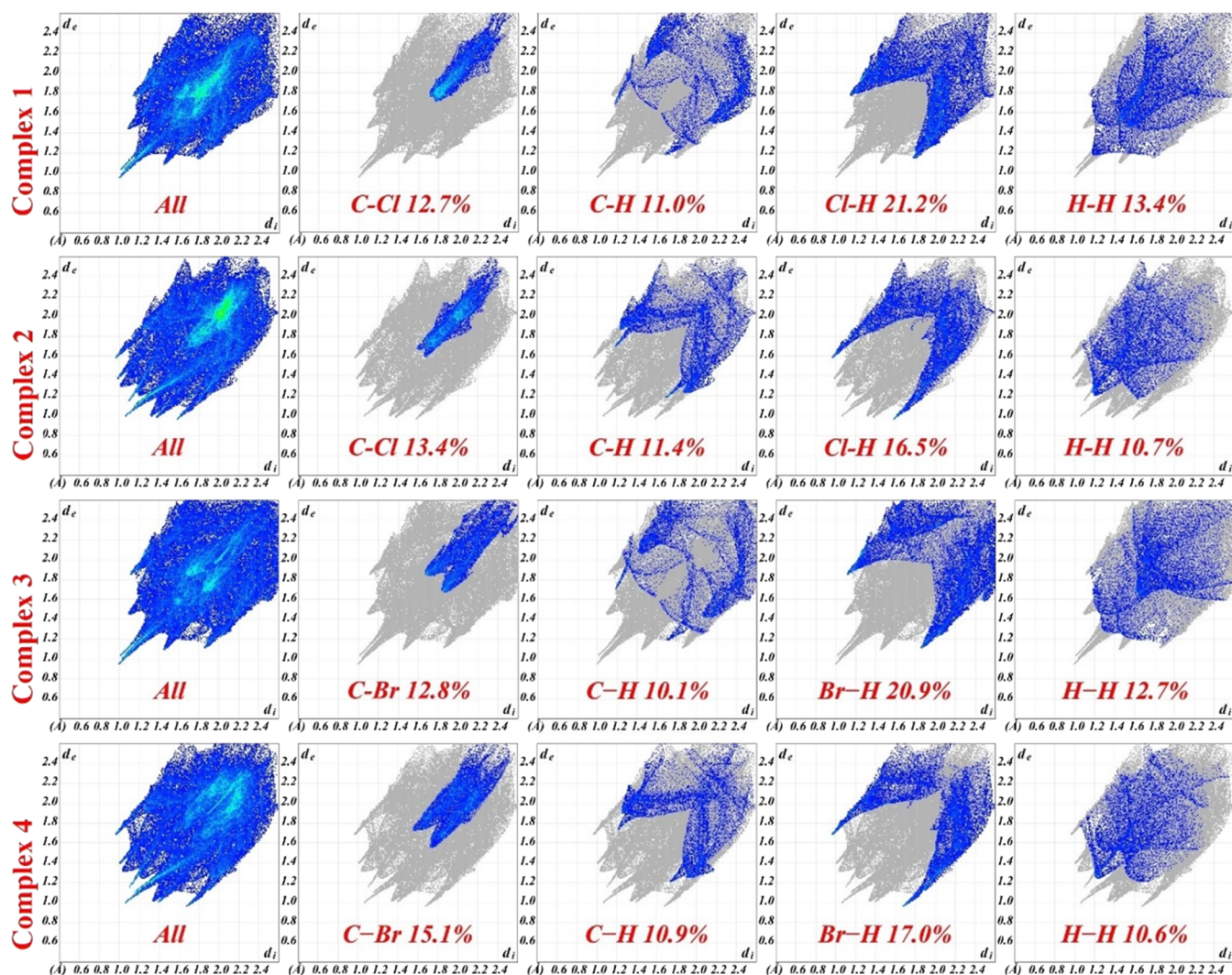


FIGURE 6 2D fingerprints of various intermolecular forces in **1–4**

TABLE 3 Hirshfeld surface calculations (%) for **1–4**

Complexes	X·H (X = Cl, Br)	H·H	C·X	C·H	N·X	N·H
1	21.2	13.4	12.7	11.0	4.3	8.5
2	16.5	10.7	13.4	11.4	8.3	8.6
3	20.9	12.7	12.8	10.1	4.1	8.4
4	17.0	10.6	15.1	10.9	8.4	7.9

with a concentration of 5×10^{-5} mol/l (Figure 7). The maximum absorption wavelength was selected as the excitation wavelength to test the fluorescence spectrum of the compounds. A 438 nm wavelength was used to excite the luminescence of a series of HL^1 , **1**, and **2** with a slit width of 2.5 nm. Upon photoexcitation at 438 nm, the free HL^1 ligand was a blue luminescent compound with the maximum at 470 nm predominantly assigned to $\pi-\pi^*$ transition fluorescence. At the same 438 nm photoexcitation, **1** and **2** exhibited also a

green luminescent emission band at 527 and 514 nm. Compared to the free ligand HL^1 , with 57 and 44 nm red-shifted for **1** and **2**, respectively, the emission at 527 and 514 nm and lower fluorescence intensity of the compounds **1** and **2** probably originated from the paramagnetic influence of Cu^{II} or Mn^{II} cations which are d^9 and d^5 ions.^[42]

As shown in Figure 7b, upon photoexcitation at 450 nm, the free HL^2 ligand exhibited a green luminescent emission peak at 512 nm predominantly also

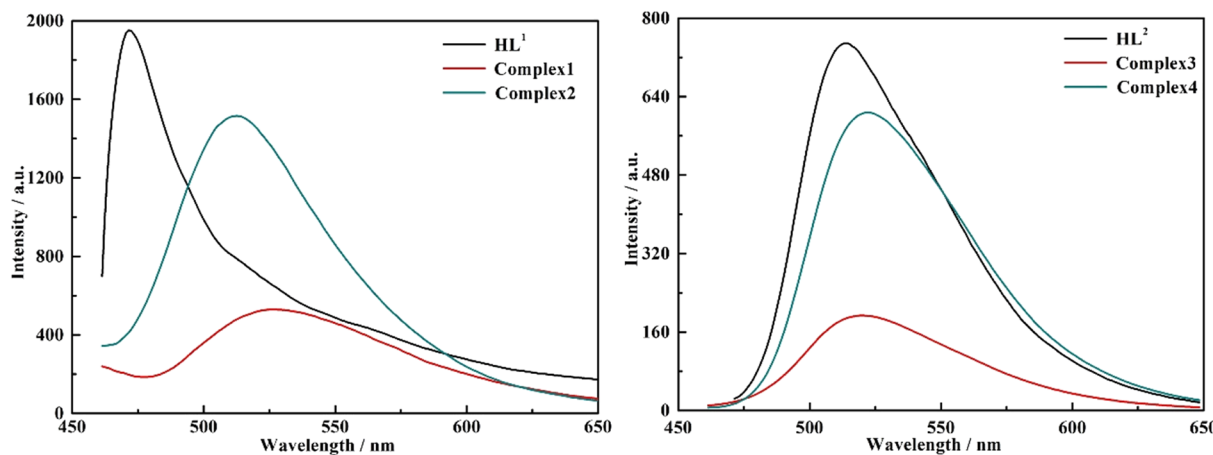


FIGURE 7 The fluorescent properties of $\text{HL}^{1\&2}$ and **1–4**

assigned to $\pi-\pi^*$ transition fluorescence. At the same 450 nm photoexcitation, **3** and **4** exhibited also a green luminescent emission peak at 519 and 522 nm. The emission peaks of **3** and **4** were red-shifted by about 7 and 10 nm for **3** and **4**, respectively, compared to the free HL^2 ligand. For **3** and **4**, lower fluorescence intensity and

redshift relative to HL^2 ligand probably originated from the paramagnetic influence of Cu^{II} or Mn^{II} cations which are d^9 and d^5 ions, respectively.^[42] By comparing the fluorescence intensity of **1** and **2** or **3** and **4**, we found that the fluorescence intensity of compounds **1** or **3** was lower than that of compounds **2** or **4** constructed with

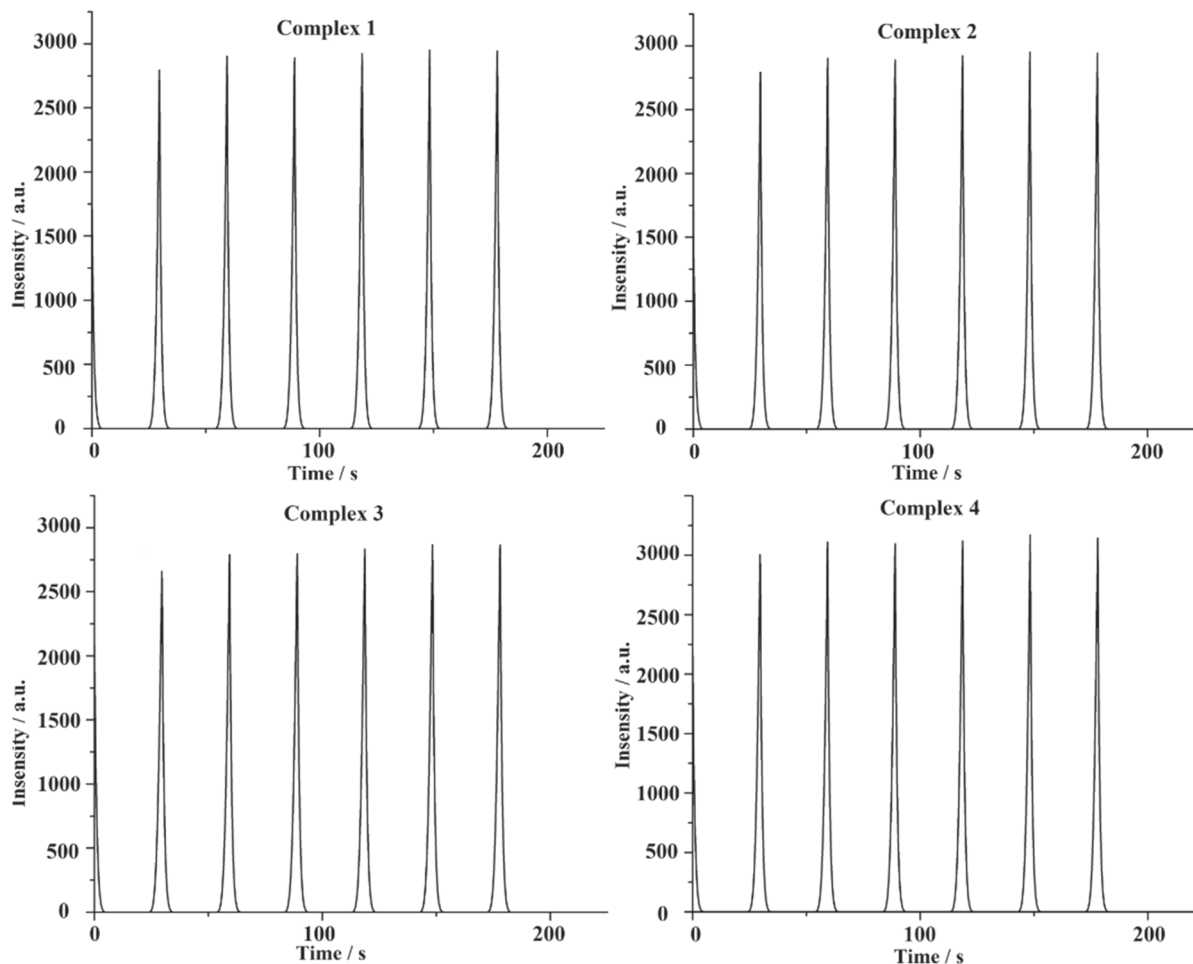


FIGURE 8 The electrochemical emission spectrum of **1–4**

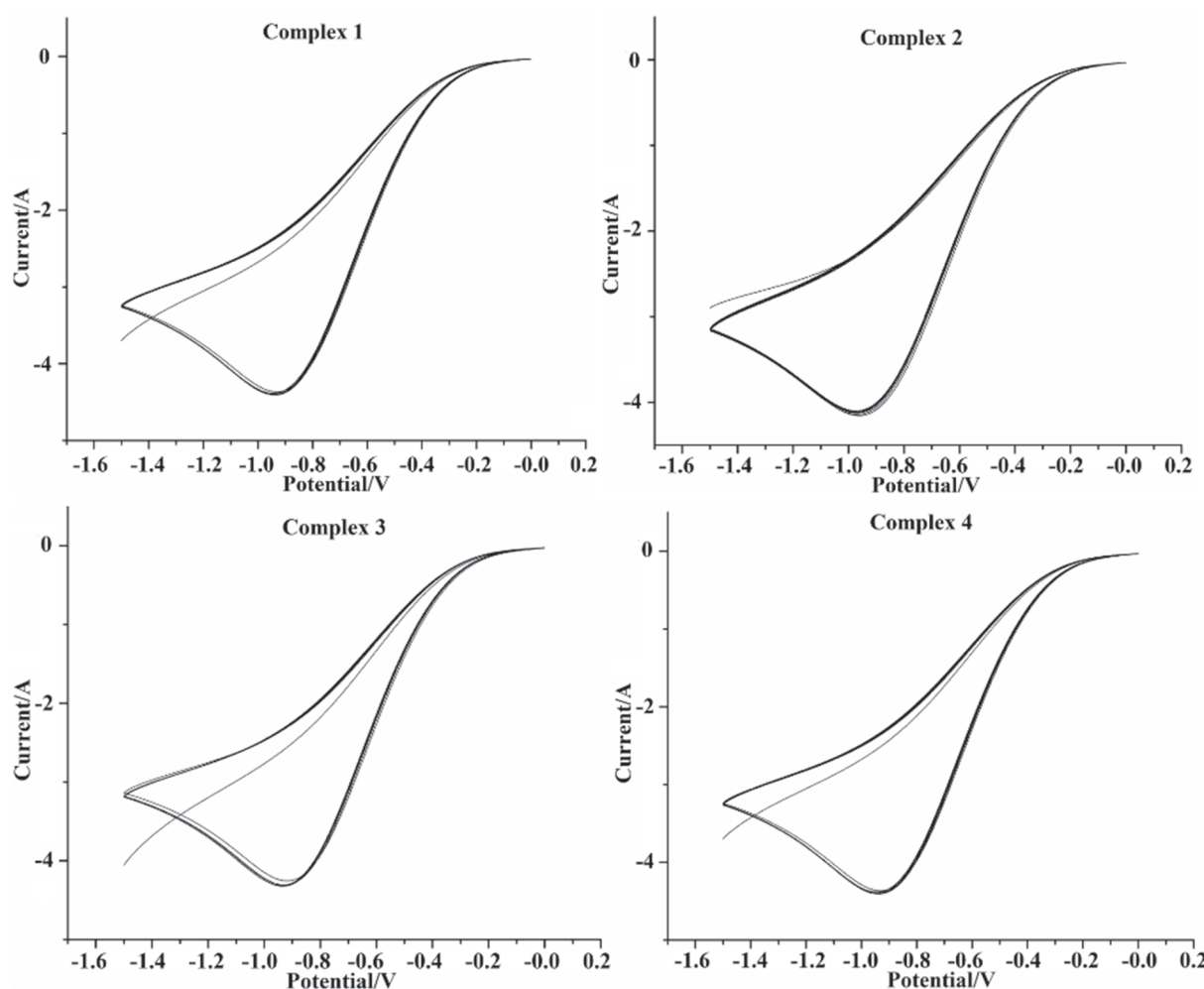


FIGURE 9 Cyclic voltammetry curves for **1–4**

the same ligand, which can be attributed to the electronegativity of the substituents and also the electron density of the ligand as the electronegativity of chlorine is greater than that of bromine. As a result, the electron density of ligand HL^1 was lower than that of ligand HL^2 , which is harmful to the ligand-to-metal charge transfer.^[30,36] The unique fluorescent properties of this series of compounds can be researched as a potential fluorescent material.

3.6 | ECL properties of **1–4**

The ECL of the pure complexes **1–4** (the phase purity of **1–4** has been checked by PXRD, Figure S4) is shown in Figure 8. CV was studied to gain insight into the redox properties of **1–4**. Figure 9 shows the experimental results of CV with glassy carbon disk electrodes modified with complexes **1–4**. For **1**, when $\text{K}_2\text{S}_2\text{O}_8$ was added to the solution, an oxidation peak in the cathodic current at -1.5 V and a reduction peak at -0.95 V in the cathodic

current were observed. The CV curves for the other three complexes are similar to that of **1**.

For complexes **1–4**, the maximum luminous intensity was about 2850, 2960, 2850, 3100 a.u., respectively. After seven circulations, the luminous intensities still maintained stability. In the different metal complexes of the same ligand, it can be found that the complex of Mn(II) has a higher maximum luminescence intensity than that of Cu(II). However, in general, these four compounds have strong and stable luminescent properties and have great potential application value in the practical application of electrochemical materials,^[39] especially compound **4**.

We have taken $[\text{Ru}(\text{bpy})_3]^3$ as a standard^[43] for the ECL yield, resulting in yields of 0.63, 0.66, 0.63, and 0.69 for complexes **1–4**, respectively. It is tentatively suggested that the introduction of the Cu and Mn ions, in particular Mn ion, could strengthen the spin-orbit coupling effect and enhance the ECL emission. Compared to Ru-, Ir-, Pt-, Re-, Os-, and Cd-complexes reported previously,^[43–45] the four complexes as novel polymer ECL materials

exhibit better economic benefits and environmental friendliness because copper and manganese are less-toxic low-priced metals.

4 | CONCLUSIONS

Four new 2D structures with Cu(II) and Mn(II) ions were successfully synthesized using two different $\text{HL}^{1\&2}$ ligands. The results of Hirshfeld surface analysis indicate that $\text{X}\cdots\text{H}$ ($\text{X} = \text{Br}, \text{Cl}$) interactions play a considerable role in stabilizing the self-assembly process. The unique fluorescent properties of **1–4** can be researched as a potential fluorescent material. In addition, complexes **1–4** possess higher stability and stronger ECL emissions and can be a useful guide for the design of novel ECL materials.

SUPPLEMENTARY INFORMATION

Crystallographic data (including structure factors) for the structures in this paper have been deposited with the Cambridge Crystallographic Data Centre as supplementary publication, with the CCDC number 1970677–1970680. Copies of the data can be obtained free of charge on application to CCDC, 12 Union Road, Cambridge CB2 1EZ, UK (fax: +44 1223 336033, email: deposit@ccdc.cam.ac.uk). Electronic supplementary information (ESI) available: Infrared curves of HL^1 , HL^2 , and **1–4** (Figure S1); interaction between 1D staircase-shaped chain (a); the 2D of **1** and **3** (b); rectangular gap of **1** and **3** (c); 3D of **1** and **3** (d) (Figure S2); the two-dimensional structure filling diagram (a) and 3D network of **2** and **4** (b, Figure S3); XRD experiments and simulation curves of **1–4** (Figure S4).

ACKNOWLEDGMENTS

Thanks to the Nature Science Foundation of China (No. 21861014), and Collaborative Innovation Center for Exploration of Hidden Nonferrous Metal Deposits and Development of New Materials in Guangxi (No. GXYSXTZX2017-II-3).

FUNDING INFORMATION

The Nature Science Foundation of China (No. 21861014) and Program of the Collaborative Innovation Center for Exploration of Hidden Nonferrous Metal Deposits and Development of New Materials in Guangxi (No. GXYSXTZX2017-II-3)

ORCID

Fanghua Ji  <https://orcid.org/0000-0002-2101-3930>

Shuhua Zhang  <https://orcid.org/0000-0002-1097-1674>

REFERENCES

- [1] S. Yuan, L. Feng, K. Wang, J. Pang, M. Bosch, C. Lollar, Y. Sun, J. Qin, X. Yang, P. Zhang, Q. Wang, L. Zou, Y. Zhang, L. Zhang, Y. Fang, J. Li, H.-C. Zhou, *Adv. Mater.* **2018**, *30*, 37.
- [2] J. Xiao, C. X. Chen, Q. K. Liu, J. P. Ma, Y. B. Dong, *Cryst. Growth Des.* **2011**, *11*, 5696.
- [3] Y. Chen, S. Zhang, Y. Xiao, S. Zhang, *Acta Cryst.* **2020**, *C76*, 236.
- [4] Y. Zhao, D. S. Deng, L. F. Ma, B. M. Ji, L. Y. Wang, *Chem. Commun.* **2013**, *49*, 10299.
- [5] E. Zhang, P. Ju, Z. Zhang, H. Yang, L. Tang, X. Hou, J. You, J. Wang, *Spectrosc. Acta A* **2019**, *222*, 117207.
- [6] G. Zhao, Y. Wang, X. Li, Q. Yue, X. Dong, B. Du, W. Cao, Q. Wei, *Anal. Chem.* **2019**, *91*, 1989.
- [7] P. Falcaro, F. Normandin, M. Takahashi, P. Scopece, H. Amenitsch, S. Costacurta, C. M. Doherty, J. S. Laird, M. D. H. Lay, T. Lisi, A. J. Hill, D. Buso, *Adv. Mater.* **2011**, *23*, 3901.
- [8] H. Tan, G. Tang, Z. Wang, Q. Li, J. Gao, S. Wu, *Anal. Chim. Acta* **2016**, *940*, 136.
- [9] R. Xiao, Y. Pan, J. Li, L. Zhang, W. Zhang, *J. Chromatogr. A* **2019**, *1601*, 45.
- [10] M. Xie, J. Tang, G. Fang, M. Zhang, L. Kong, F. Zhu, L. Ma, D. Zhou, J. Zhan, *J. Hazard. Mater.* **2020**, *384*, 121345.
- [11] Z. Wang, H. Yu, J. Han, G. Xie, S. Chen, *Chem. Commun.* **2017**, *53*, 9926.
- [12] F. A. A. Paz, J. Klinowski, S. M. Vilela, J. P. Tome, J. A. Cavaleiro, J. Rocha, *Chem. Soc. Rev.* **2012**, *41*, 1088.
- [13] X. G. Yang, X. M. Lu, Z. M. Zhai, Y. Zhao, X. Y. Liu, L. F. Ma, S. Q. Zang, *Chem. Commun.* **2019**, *55*, 11099.
- [14] L. Ma, C. Abney, W. Lin, *Chem. Soc. Rev.* **2009**, *38*, 1248.
- [15] D. Yang, B. C. Gates, *ACS Catal.* **2019**, *9*, 1779.
- [16] V. V. Dhayabaran, T. D. Prakash, R. Renganathan, E. Friehs, D. W. Bahnemann, *J. Fluoresc.* **2017**, *27*, 135.
- [17] Y. Gong, T. Wu, P. G. Jiang, J. H. Lin, Y. X. Yang, *Inorg. Chem.* **2013**, *52*, 777.
- [18] H. Liang, Y. Q. Zhou, P. W. Shen, *Chin. Sci. Bull.* **1994**, *39*, 1452.
- [19] H. Park, G. Kringsfeld, S. J. Teat, J. B. Parise, *Cryst. Growth Des.* **2007**, *7*, 1343.
- [20] L. Sun, H. Chen, C. Ma, C. Chen, *Inorg. Chem. Commun.* **2017**, *77*, 77.
- [21] Y. Xu, X. B. Yin, X. W. He, Y. K. Zhang, *Biosens. Bioelectron.* **2015**, *68*, 197.
- [22] D. Feng, X. Tan, Y. Wu, C. Ai, Y. Luo, Q. Chen, H. Han, *Biosens. Bioelectron.* **2019**, *129*, 100.
- [23] G. B. Hu, C. Y. Xiong, W. B. Liang, X. S. Zeng, H. L. Xu, Y. Yang, L. Y. Yao, R. Yuan, D. R. Xiao, *ACS Appl. Mater. Interfaces* **2018**, *10*, 15913.
- [24] X. Yang, Y. Q. Yu, L. Z. Peng, Y. M. Lei, Y. Q. Chai, R. Yuan, Y. Zhuo, *Anal. Chem.* **2018**, *90*, 3995.
- [25] J.-M. Wang, Q.-J. Deng, S.-H. Zhang, *Chin. J. Struct. Chem.* **2020**, *39*, 118.

- [26] X. Shen, T. Zhang, S. Broderick, K. Rajan, *Mol. Syst. Des. Eng.* **2018**, *3*, 826.
- [27] X. Zheng, M. Yi, Z. Chen, Z. Zhang, L. Ye, G. Cheng, Y. Xiao, *Appl. Organomet. Chem.* **2020**, *34*, e5584(), -. <https://doi.org/10.1002/aoc5584>
- [28] D. Kojima, T. Sanada, N. Wada, K. Kojima, *RSC Adv.* **2018**, *8*, 31588.
- [29] P. Chandrasekhar, A. Mukhopadhyay, G. Savitha, J. N. Moorthy, *Chem. Sci.* **2016**, *7*, 3085.
- [30] T. Yanagimoto, A. Nakagawa, T. Komatsu, E. Tsuchida, *Bull. Chem. Soc. Jpn.* **2001**, *74*, 2123.
- [31] A. Yadav, A. K. Srivastava, A. Balamurugan, R. Boomishankar, *Dalton Trans.* **2014**, *43*, 8166.
- [32] O. V. Dolomanov, L. J. Bourhis, R. J. Gildea, J. A. K. Howard, H. Puschmann, *J. Appl. Cryst.* **2009**, *42*, 339.
- [33] G. M. Sheldrick, *Acta Crystallogr.* **2015**, *C71*, 3.
- [34] G. M. Sheldrick, *Acta Crystallogr.* **2008**, *A64*, 112.
- [35] S. H. Zhang, R. X. Zhao, G. Li, H. Y. Zhang, Q. P. Huang, F. P. Liang, *J. Solid State Chem.* **2014**, *220*, 206.
- [36] M. A. Halcrow, *Chem. Soc. Rev.* **2013**, *42*, 1784.
- [37] S. M. Zhang, H. Y. Zhang, Q. P. Qin, J. W. Fei, S. H. Zhang, *J. Inorg. Biochem.* **2019**, *193*, 52.
- [38] C. Wu, X. Zheng, G. Chen, Z. Chen, Y. Xiao, *J. Cluster Sci.* **2019**, *30*, 1347.
- [39] H.-Y. Zhang, Y. Xiao, Y. Zhu, *Chinese J. Struct. Chem.* **2017**, *36*, 848.
- [40] M. Shebl, *Spectrochim. Acta* **2014**, *117*, 127.
- [41] J. J. McKinnon, M. A. Spackman, A. S. Mitchell, *Acta Crystallogr.* **2004**, *B60*, 627.
- [42] I. E. Mikhailov, N. I. Vikrishchuk, L. D. Popov, G. A. Dushenko, A. D. Beldovskaya, Y. V. Revinskii, V. I. Minkin, *Russ. J. Gen. Chem.* **2016**, *86*, 1054.
- [43] M. M. Richter, *Chem. Rev.* **2004**, *104*, 3003.
- [44] B. M. Huang, X. B. Zhou, Z. H. Xue, X. Q. Lu, *TrAC Trends Anal. Chem.* **2013**, *51*, 107.
- [45] Y. Zhou, W. Li, L. Yu, Y. Liu, X. Wang, M. Zhou, *Dalton Trans.* **2015**, *44*, 1858.

SUPPORTING INFORMATION

Additional supporting information may be found online in the Supporting Information section at the end of this article.

How to cite this article: Zeng Y, Zhang H, Zhang Y, Ji F, Liang J, Zhang S. Synthesis, crystal structures, fluorescence, electrochemiluminescent properties, and Hirshfeld surface analysis of four Cu/Mn Schiff-basecomplexes. *Appl Organomet Chem.* 2020;e5712. <https://doi.org/10.1002/aoc.5712>